Cement and Concrete Research 130 (2020) 106010

Contents lists available at ScienceDirect

Cement and Concrete Research

journal homepage: www.elsevier.com/locate/cemconres

Simulation of chloride diffusion in fly ash and limestone-calcined clay cement (LC^3) concretes and the influence of damage on service-life

Pu Yang[a], Yuvaraj Dhandapani[b], Manu Santhanam[c], Narayanan Neithalath[d,*]

[a] School of Sustainable Engineering and the Built Environment, Arizona State University, Tempe, AZ, United States of America
[b] Department of Civil Engineering, Indian Institute of Technology Madras, Chennai, India
[c] Department of Civil Engineering, Indian Institute of Technology Madras, Chennai, India
[d] School of Sustainable Engineering and the Built Environment, Arizona State University, Tempe, AZ, United States of America

ARTICLE INFO

Keywords:
Chloride transport
Tortuosity
Chloride binding
Modeling
Damage parameter

ABSTRACT

Numerical simulation of chloride diffusion through high-performance binding systems such as limestone-calcined clay cement (LC^3) and its comparison to control and fly ash modified concretes is discussed. The simulation framework considers the pore structure of concrete, the concentration-dependence of diffusion coefficient, and Freundlich binding. The LC^3 concrete and the companion fly ash concrete exhibit similar service lives (~8× control mixture), despite the LC^3 system having a reduced clinker factor than the fly ash concrete (~0.5, as opposed to 0.7). The diffusion model is augmented with a scalar isotropic damage variable that accounts for random distribution of microcracks under fatigue loading (e.g., in a bridge deck). The impact of damage on service life at different stress levels, for the different concretes is elucidated. The modeling approach can be used to evaluate the influence of binder composition and damage on effective service life of chloride-exposed concrete structures, thereby aiding in binder selection.

1. Introduction

Chloride-induced steel reinforcement corrosion and the consequent reduction in service life of concrete structures is a major concern all over the world. A recent report has identified that about 3.4% of the global GDP (amounting to about $2.5 trillion USD) is spent annually to prevent, mitigate and repair civil infrastructure damaged due to chloride-induced corrosion [1]. The transport of chloride ions through concrete occurs through diffusion, permeation, capillary suction, or migration. Diffusion, described by Fick's law, is generally considered to be the dominant mechanism in field concretes subjected to long-term exposure, where a chemical potential drives the free Cl^- ions towards areas of lower Cl^- concentration. Long-term test methods such as the one prescribed in ASTM C 1556 are used to determine the Cl^- transport properties in such cases. When the Cl^- ion transport is electrically accelerated through application of an external potential, the presence of other electrically mobile ions in the pore solution induces electrical migration of ions. The ionic flux can be rigorously defined using the Nernst-Planck equation [2–4] which describes the distribution and evolution of the electrical field in concrete in the case of electrically accelerated ionic transport [5–8]. The flux, in electrically accelerated transport, is due to a combination of diffusion and migration processes (ignoring convective effects, i.e., no pressure or moisture gradients). For each ionic species, a separate conservation equation is used, along with the imposition of Poisson's equation (thus making it the Poisson-Nernst-Planck equation [5,6]), which couples the transport of individual ions. The migration rate depends on the electric field strength and the ion mobility. Neglecting the migration term for practical exposure conditions, ionic transport can be conveniently expressed using Fick's law. The transport is thus controlled by the diffusion coefficient.

The diffusion coefficient is significantly influenced by the pore structure of the diffusing medium. This has led to a large body of work on the use of supplementary cementing materials (SCMs) that densify the pore structure and thereby retard the diffusion of Cl^- [9]. In addition, some of these SCMs also contribute to Cl^- ingress retardation through chloride binding [10–14]. Of late, binders with a combination of SCMs and reactive fillers are gaining attention in view of their beneficial synergies. One such multiple-blend binder system utilizes the synergy of limestone powder with alumina-rich SCMs such as fly ash, slag, and calcined clays [15–21]. This approach, in addition to decreasing the burden on clinker content, compensates for the loss in early age strength observed in high volume replacement of cement with SCMs such as fly ash [22]. Recent studies on limestone-calcined clay cement (LC^3) concretes have shown mechanical performance

* Corresponding author.
E-mail address: Narayanan.Neithalath@asu.edu (N. Neithalath).

https://doi.org/10.1016/j.cemconres.2020.106010
Received 5 May 2019; Received in revised form 2 January 2020; Accepted 4 February 2020

comparable to that of ordinary Portland cement concrete even at low clinker factors, and significantly enhanced durability performance [23–26].

The objective of this paper is to develop and demonstrate a numerical framework with explicit considerations of the pore structure, concentration-dependence of diffusion coefficient, and chloride binding to describe the chloride transport through LC^3 and fly ash concretes. Furthermore, to better understand Cl^- transport in infrastructure (e.g., bridges) under in-service (fatigue) conditions, a scalar damage parameter based on Miner's rule is implemented in the simulations. It is expected that such comprehensive simulation strategies can be used to evaluate the influence of a range of microstructural and chemical parameters, which when related to the binder composition, aids in the design of durable and sustainable concretes.

2. Simulation approach

The steady-state ionic flux (J; mol/m^2/s) through a saturated porous medium such as concrete (i.e., under no external electrical potential) can be defined using the ionic concentration gradient as:

$$J = -D_{eff}\left(\frac{\partial C}{\partial x}\right) \tag{1}$$

C is the ionic concentration in the pore solution (mol/m^3), and D_{eff} is the effective diffusion coefficient of chloride ions through concrete (m^2/s), defined as:

$$D_{eff} = \frac{\phi}{\tau^2} D_{inf} = \phi D_0 \tag{2}$$

Here, D_{inf} is the diffusion coefficient of the considered ion at infinite dilution, equal to 2.03×10^{-9} m^2/s for Cl^- [5], D_0 is the diffusion coefficient through the infinitely dilute pore solution, ϕ is the porosity, and τ is the geometric tortuosity of the pore network, defined as the ratio of the length of the transport path (l_{path}) to the shortest distance between the start and end points of the path (L) [27]. The scaling of diffusive transport with the inverse square of tortuosity has been reported for many porous systems, and a rigorous derivation can be found in [28]. The tortuosity as described here is an electrical tortuosity (see the Test methods section below), and thus can be considered to account for the pore constrictivity also since the electrical flow lines in a pore adjust to changing cross-sectional dimensions [29]. In materials with complex pore structure such as concrete, tortuosity is difficult to directly measure, and hence it is taken to be a function of the pore connectivity (β) obtained from electrical conductivity measurements. The pore connectivity is related to the tortuosity of the pore network as shown below [5,30]:

$$\tau = \frac{1}{\sqrt{\beta}} \tag{3}$$

A part of the chlorides diffusing through concrete can be bound in the hydration products. Chloride binding influences the transport process significantly, and thus is an important determinant of the service-life of chloride-exposed reinforced concrete structures [31–34]. While it is well understood that chlorides can be chemically bound to the hydration products (e.g., to form Friedel's salt; irreversible binding) or physically adsorbed on the product surfaces (reversible binding), it is difficult to practically distinguish between them. Thus, the experimentally determined total bound chloride content is generally used. The free chlorides (those present in the pore solution) travel through the porous medium, and in time, result in depassivation of reinforcing steel.

The relationship between free and bound chlorides is non-linear, and is described using binding isotherms, the common ones being the Langmuir and Freundlich isotherms [10,33]. The ranges of Cl^- concentration in the pore solution for which these isotherms are applicable are provided in [33]. Based on previous work [35,36] and experimental results, Freundlich isotherm is used in this work, represented as:

$$C_b = k_b C^m \tag{4}$$

C_b (mol/kg of solid) and C (mol/m^3 of liquid) are the bound and free chloride concentrations, and k_b and m are the binding coefficients. k_b has units consistent with those of C_b and C, and m is unitless.

Since mass transport is considered to occur through the pore phase only, and chloride binding occurs only in the solid phase, mass conservation is described as follows:

$$\frac{\partial(\phi C)}{\partial t} + (1-\phi)\rho_c \frac{\partial C_b}{\partial t} = -\frac{\partial J}{\partial x} = D_{eff}\frac{\partial}{\partial x}\left(\frac{\partial C}{\partial x}\right) \tag{5}$$

Here, ρ_c is the density of concrete (taken as 2400 kg/m^3).

Binding of chloride ions in the hydrated phases can be expressed using a first order reaction term (r), such that:

$$(1-\phi)\rho_c \frac{\partial C_b}{\partial t} = r \tag{6}$$

The reaction term that defines the mass transfer of chlorides can be treated as a function of a reaction rate constant (κ) and the difference in Cl^- concentration between the pore solution (C) and the solid-liquid interface (C_i) that drives the binding process [4][1].

$$r = \kappa(C - C_i) \tag{7}$$

The chloride concentration in the liquid-solid interface (C_i) for non-equilibrium conditions can be calculated from the Freundlich isotherm by replacing the ionic concentration in the bulk pore solution (C) with C_i as shown in Eq. (8). Note that, for a given time step, $C_i < C$.

$$C_i = \left(\frac{C_b}{k_b}\right)^{1/m} \tag{8}$$

Hence the continuity equation (Eq. (5)) can be formulated as a system of equations as:

$$\frac{\partial(\phi C)}{\partial t} - D_{eff}\frac{\partial}{\partial x}\left(\frac{\partial C}{\partial x}\right) = -\kappa\left[C - \left(\frac{C_b}{k_b}\right)^{1/m}\right]$$

$$(1-\phi)\rho_c \frac{\partial C_b}{\partial t} = \kappa\left[C - \left(\frac{C_b}{k_b}\right)^{1/m}\right] \tag{9}$$

D_{eff} in Eq. (9) considers only the influence of pore structure on diffusion. In reality, chloride ions diffuse through an ion-enriched pore solution, and not an infinitely dilute solution. The relationship between D_i and D_{inf} can be stated as [2,5]:

$$D_i = D_{inf}\frac{\lambda_i}{\lambda_i^0} \tag{10}$$

λ_i is the equivalent conductivity of the ionic species i, and λ_i^0 is its equivalent conductivity at infinite dilution. λ_i for a certain ionic species is a function of λ_i^0, ionic strength of the solution, and the conductivity coefficient for the relevant ionic species. Ionic strength accounts for concentration of all the ionic species in the pore solution, which can be obtained from pore solution extraction experiments [37,38] or obtained from a simplified web interface developed by NIST [39]. More details can be found in [40]. Such a formulation has been implemented in the numerical simulation of non-steady state chloride migration test [5]. Thus, D_{eff} in Eq. (9) can be stated as:

$$D_{eff} = \frac{\phi}{\tau^2}\frac{\lambda_i}{\lambda_i^0} D_{inf} \tag{11}$$

The use of concentration-dependent diffusion coefficients induces a

[1] Instead of C-C$_i$, one can also use the difference between the equilibrium bound chloride and the amount of chlorides bound at a given time as the driving force for binding. Eq. (8) then becomes: $r = \kappa(C_b - k_b C^m)$.Both formulations are identical.

retardation effect on the ionic transport process.

Eq. (9) was solved using two different finite element models – one using a custom developed MATLAB program incorporating built-in PDE solvers for one-dimensional transport, and the other using the commercial multiphysics environment, COMSOL, for two-dimensional transport. In general, a 1D model is sufficient to define chloride ion transport through bulk concrete. When inhomogeneities that influence transport such as cracks, interfacial transition zone etc. needs to be accounted for, 2D or 3D models become necessary. This paper mostly uses a 1D model, though comparisons with a 2D model are shown for select cases. For the 1D simulations, a 100 mm thick specimen was used, discretized to 1000 nodes along the depth. The exposure solution was assigned to the upstream node as a constant surface concentration while a free Cl^- concentration of zero was assigned to the downstream node. The uniform Cl^- concentration in the sample (obtained from companion experiments) were assigned to all the nodes. The free Cl^- concentration at each node was used to update the equivalent conductivities from which concentration-dependent diffusion coefficients were determined. This approach also ensures time-dependence of diffusion coefficient in the simulations. The time-dependence mentioned here is due to the concentration-time relationship and not due to maturing concrete. It is assumed that there are no hydration reactions that alter the microstructure further since all the transport tests in this paper are carried out after 1 year of curing.

The 2D model developed in COMSOL accounts for the presence of aggregates in the mixture also. Here, we consider 50% of aggregates in the concrete, by volume, with 10 mm and 20 mm coarse aggregates in a 2:3 ratio. Since the 2D model is used in this paper only to show that an accurate 1D model is sufficient to estimate of transport in the absence of cracking, the actual aggregate contents (~65% by volume), which would slightly impact the depth-dependent ionic concentrations, are not considered. The numerical specimen with 100 mm sides and random aggregate distribution was created using a MATLAB program. A zero-flux condition was imposed on the side boundaries.

3. Experimental program

3.1. Materials and mixtures

Ordinary portland cement (OPC; conforming to IS 269/ASTM C 150) was used to fabricate the concrete mixtures. A Class F fly ash was used in certain mixtures to replace 30% of the OPC by mass. LC^3 was obtained from a trial industrial production in India, and had a composition of 31% calcined clay and 15% limestone. A locally sourced clinker was blended with limestone and calcined clay to produce LC^3, the details of which can be found in [41]. The chemical composition of OPC, fly ash, and the components of the LC^3 system are shown in Table 1. A graded river sand with a 4.75 mm nominal maximum size, and a mixture of 10 mm and 20 mm sized crushed granite in a 40:60 ratio were used as the aggregates. A polycarboxylate ether-based superplasticizer with a solids content of 34% was used to achieve the target slump of 80–120 mm. The mixtures were designed for two different compressive strengths (30 MPa and 50 MPa) by adjusting the binder and water contents. The numbers 30 and 50 in the mixture designations indicate the design compressive strengths, and are termed as the A and B series mixtures respectively. Mean 28-day cube compressive strengths of 38 ± 5 MPa and 60 ± 5 MPa were fixed as the acceptable targets for the chosen strength grades. To facilitate comparison, control concrete mixtures (C series) with same binder content and water-to-binder ratio (w/b) (360 kg/m^3 and 0.45) were also designed. The details of the concrete mixtures used in this paper are shown in Table 2. The specimens were cured for a period of 1 year in a moist chamber (> 95% RH, 25 ± 2 °C).

3.2. Test methods

3.2.1. Diffusion experiments and determination of chloride binding

Bulk diffusion experiments in accordance with ASTM C 1556 were carried out on the concrete specimens cured for 1 year in a moist environment. The bulk diffusion experiments were carried out on 100 mm long × 100 mm diameter cylindrical specimens for a duration of 56 days. The specimens were epoxy coated with only a 100 mm diameter face exposed, and immersed in a 2800 mol/m^3 NaCl solution. Chloride profiles were obtained by sampling the concrete powder extracted at several depths from the surface (up to 25 mm). The powder was tested for acid-soluble chlorides to estimate the total chloride content as a function of depth, and water-soluble chlorides to estimate the free chloride concentration. Freundlich isotherm was used to relate the bound chloride content (the difference between the total and free chloride contents) and the free chloride content.

3.2.2. Porosity and tortuosity

Concrete cores of 70 mm diameter were extracted from 150 mm cubical specimens after the desired curing duration. The surface of the cores was epoxy coated and sliced into four approximately 30 mm thick discs after discarding the top and bottom 5 mm of the core. The specimens were conditioned in an oven at 50 °C for 7 days and subjected to vacuum saturation in accordance with ASTM C1202. The mass of the saturated and oven dried specimens were used to determine the water accessible porosity (ϕ).

Bulk effective electrical conductivity (σ_{eff}) of the specimens was determined in accordance with ASTM C 1760 after 1 year of moist curing. Pore solutions were extracted from companion cement pastes [38] and analyzed using inductively coupled plasma optical emission spectroscopy (ICP-OES) to determine the ionic concentrations. The concentrations of Ca^{2+}, K^+, and Na^+ thus obtained, along with the OH^- ion concentrations obtained by imposing the electrical neutrality condition were used to determine the pore solution conductivity (σ_{pore}) as described in [40]. The pore connectivity factor (β) was estimated by normalizing the bulk conductivity with the pore solution conductivity and dividing it by the porosity [30]. The ratio of pore solution conductivity to the bulk conductivity is commonly called the formation factor. The tortuosity was calculated from β using Eq. (3). A rigorous derivation of this relationship between τ and β, where pores of a uniform size are assumed for simplicity, can be found in [5].

Table 1
Chemical composition of the binding materials used in this study.

Source materials		Oxide composition (% by mass)								
		CaO	SiO_2	Al_2O_3	Fe_2O_3	MgO	Na_2O	K_2O	SO_3	LOI
OPC		64.59	19.01	4.17	3.89	0.88	0.16	0.59	1.70	1.40
Fly ash		1.28	59.32	29.95	4.32	0.61	0.16	1.44	0.16	–
LC^3	Clinker	63.81	21.12	5.24	3.41	3.06	0.32	0.19	0.63	0.98
	Calcined clay	0.09	54.83	24.95	5.08	0.19	0.05	0.21	–	9.58
	Limestone	48.54	10.07	1.74	1.62	0.47	–	0.13	0.01	37.09

Table 2
Mixture proportions of the concretes used in this study.

Mix/Strength grade	Mix ID	w/b	Cement	Fly ash	Water	Fine aggregate	Coarse aggregate	Superplasticizer (% by wt. of binder)
			kg/m^3					
Control (C)	FA-C	0.45	252	108	162	721	1157	0.23
	LC^3-C	0.45	360	–	162	687	1191	0.36
30 MPa (A)	OPC-30	0.50	310	–	155	695	1240	0.02
	LC^3–30	0.50	310	–	155	708	1227	1.0
50 MPa (B)	OPC-50	0.40	360	–	144	703	1193	0.65
	FA-50	0.35	266	114	133	699	1188	0.60
	LC^3–50	0.40	340	–	136	704	1220	0.85

4. Results and discussions

4.1. Application of numerical simulation to experimental results

The experimental chloride concentration profiles of the seven concrete mixtures shown in Table 2 belonging to plain OPC concrete, concrete with 30% of OPC (by mass) replaced by fly ash, and LC^3 concrete were modeled using Eq. (9). Porosity, tortuosity, and the binding coefficients (k_b and m) obtained from experiments described above were used in the simulations. Based on the porosity and tortuosity, the effective diffusion coefficients (D_{eff}) were obtained using Eq. (2), and corrected to establish concentration-dependence (Eq. (11)). The reaction rate constant (κ) was used as a fitting parameter in the equation since it is difficult to experimentally determine.[2] Previous work on non-steady state migration has used κ values in the range of 10^{-6}/s for cementitious binders of varying w/c and supplementary cementing materials type and content [42], and 10^{-7}/s for mortars subjected to natural diffusion [43]. Thus, the initial values for κ for simulations was chosen in the range of 10^{-8}/s since the rate constant under natural diffusion in concretes can be considered to be lower than those in mortars or under electrically accelerated conditions.

Fig. 1(a) and (b) depict the experimental total chloride contents by mass of concrete as a function of penetration depth for specimens subjected to natural diffusion (bulk diffusion tests) for 56 days after 1 year of curing, and the simulation results obtained from the solution of Eq. (9). The former shows the results for the control and 30 MPa mixtures (A series), while the latter shows the results for the 50 MPa mixtures (B series). It can be noted that the input parameters from the experiments along with a coupled reaction-transport model (binding-diffusion) adequately describes the transport of chloride ions through mature, compositionally different systems exposed to the bulk diffusion test. The values of porosity, tortuosity, baseline chloride concentration, and the Freundlich chloride binding coefficients determined from experiments, along with the rate constants that provided adequate model fits are shown in Table 3. The input effective diffusion coefficients are functions of the microstructure (based on Eq. (2)) and its concentration-dependent values are calculated within the simulations. Fig. 1(c) depicts the chloride profile bands for the B series mixtures, after accounting for the uncertainties in the input parameters shown in Table 3. Note that the variabilities in ϕ and τ will automatically be reflected in the values of D_{eff} (see Eqs. (2) and (11)). Since D_{eff} is related to $\frac{\phi}{\tau^2}$, the maximum value of ϕ for a certain mixture is paired with the minimum value of τ (based on the standard deviations provided in Table 3) and vice versa to ensure the use of extremum values of D_{eff} in the simulations.

It must be noted that the continuity equation uses the time derivative of ϕC (rather than C used for bulk diffusion calculations using Fick's law); thus the effective diffusivities reported in Table 3 *theoretically* differ from the measured bulk diffusivities by a factor ϕ. For instance, the diffusion coefficients of the concretes measured from experimentally determined chloride profiles vary from 1.3×10^{-12} m^2/s to 18.7×10^{-12} m^2/s [26] and the effective diffusion coefficients used for simulations in Table 3 (which are functions of the pore structure alone) vary from 0.23×10^{-12} m^2/s to 2.65×10^{-12} m^2/s, based on the mixture composition. Note that, when chloride binding (which is a function of the reaction product chemistry) and concentration dependence of diffusion coefficient are considered, it is fair to assume that no definitive relationships can be sought between the actual diffusivities of the material (which changes with simulation time) and the effective diffusivities used as inputs.

The one-dimensional reaction-transport model considers the diffusing medium to be homogeneous. A 2D or 3D model is required to incorporate the influence of heterogeneities such as transverse cracks, interfacial transition zones (ITZ) between the paste and aggregates, or porous aggregates on ionic transport [43–46]. A 2D model that was developed in COMSOL to study the effect of transverse cracking and paste-aggregate interfaces (not discussed in this paper) is used here for comparison with the outputs of the 1D model. Here, the aggregates are considered as impermeable inclusions in the matrix, perfectly bonded to the cement paste. Fig. 2 shows the depth-dependent total chloride contents for the 30 MPa OPC concrete specimen (A series) subjected to bulk diffusion, simulated using both the 1D (in MATLAB) and 2D (in COMSOL) models. The predicted chloride profiles are very similar for both the cases, justifying the use of a 1D model.

4.1.1. Modifications to measured tortuosity

In order to ensure appropriate fits in Fig. 1, the tortuosity values of the LC^3 mixtures had to be reduced by around 10–20% from the experimentally measured values, as shown in Fig. 3. This can be attributed to the foundational differences in tortuosity measurement and the actual transport process that is controlled by the pore tortuosity. The exact meaning of tortuosity differs in the context of different transport phenomena [5,47,48]. In this case, tortuosity is determined from experimentally measured electrical conductivities; i.e., the transport process employed in tortuosity measurement relies on the electrical path lengths. While ionic diffusion and electrical conduction are closely related phenomena, both of which are solved by Laplace equations describing a scalar field of ionic concentration or charge, it has been noticed that a discrepancy of about 10% is observed between electrical and diffusional tortuosities [47], similar to the observations in this paper. The difference is more pronounced when the pore structure is highly refined, as is noticed for LC^3 concretes. One plausible reason is postulated as follows: the electrical tortuosity determined from conductivity also accounts for the pore constrictions (or pore throats). Since the pore structure is generally more constricted when it is refined, a higher electrical tortuosity results. However, all of those constrictions might not be impediments to the ionic diffusion path, likely rendering the diffusion tortuosity to be lower than the electrical tortuosity for such a system. Past work has shown that the pore structure of LC^3

[2] If, only the experimental chloride profile from ASTM C 1556 test is available, the model could be used on this profile, along with an error minimization scheme with appropriate bounds to directly estimate the effective diffusion coefficient, binding parameters, and the rate constant.

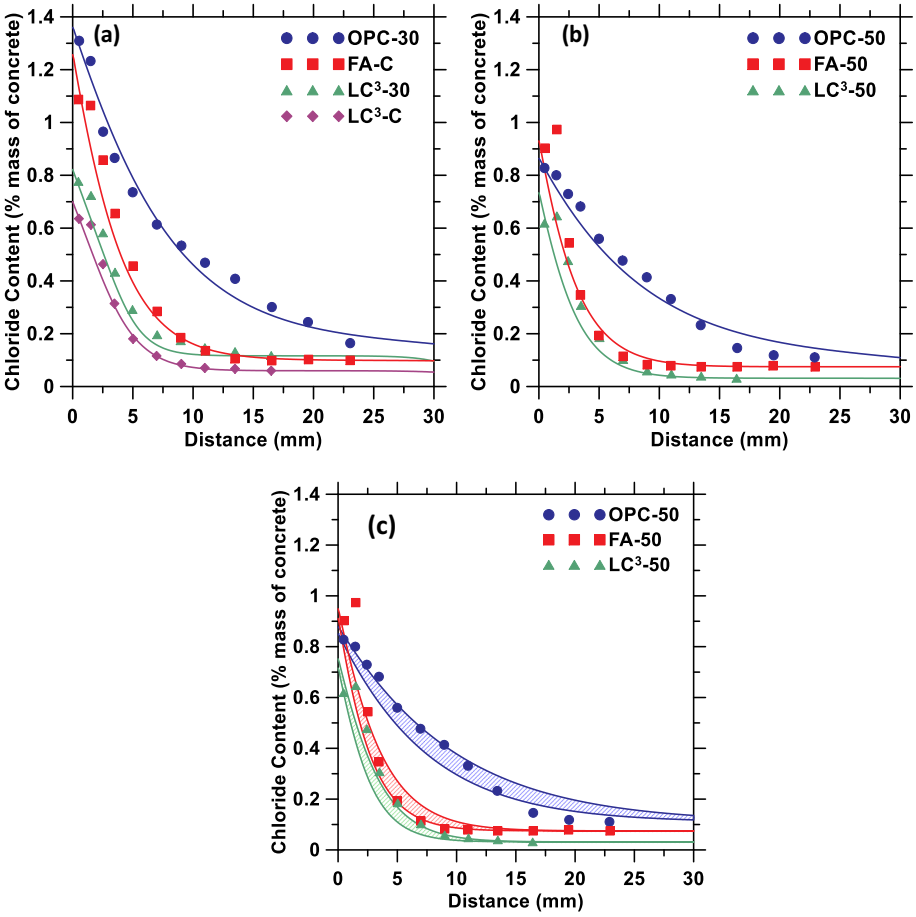

Fig. 1. Total chloride profiles after 56 days of simulation for: (a) Series A (30 MPa) and C (control) mixtures, (b) series B (50 MPa) mixtures, and (c) the uncertainties in chloride profiles for the series B mixtures, after accounting for standard deviations of input data shown in Table 3. The solid lines in (a) and (b) correspond to the simulation, based on the mean values of input parameters shown in Table 3.

Table 3
Input parameters for the numerical simulation model.

Mix/Strength grade	Mix ID	w/b	Porosity (ϕ)	Tortuosity (τ)	Base-line Cl^- (C_{bo}), mg/g	Freundlich binding coefficients		Rate constant (κ), $\times 10^{-8}$ 1/s	Mean effective diffusion coefficient[a] (D_{eff}), $\times 10^{-12}$ m^2/s
						K_b	m		
Control (C)	FA-C	0.45	0.069 ± 0.002	14.5 ± 1.62	0.99	8.62	0.39	5.00	0.66
	LC^3-C	0.45	0.097 ± 0.007	24.5 ± 1.91	0.60	2.59	0.39	3.50	0.33
30 MPa (A)	OPC-30	0.50	0.076 ± 0.003	7.60 ± 1.15	1.64	9.29	0.34	5.00	2.65
	LC^3–30	0.50	0.100 ± 0.01	28.5 ± 2.12	1.17	2.95	0.31	7.00	0.25
50 MPa (B)	OPC-50	0.40	0.062 ± 0.003	7.50 ± 0.83	1.10	7.36	0.33	2.50	2.25
	FA-50	0.35	0.069 ± 0.004	21.0 ± 2.40	0.75	6.43	0.29	3.00	0.32
	LC^3–50	0.40	0.052 ± 0.004	21.8 ± 1.96	0.32	4.28	0.42	3.00	0.23

[a] These values consider only the pore structure effect and are directly calculated from Eq. (2). However, the solution of Eq. (9) implicitly accounts for concentration-dependence through Eq. (11). The values given here are the mean values based on the mean values of ϕ and τ, the variabilities of which are shown in this table.

pastes is highly refined as compared to OPC and fly ash-bearing systems, even at early ages [25]. This is on account of the increased early-age reactivity of the calcined clays or such aluminosilicates as compared to Class F fly ash, as reported in [20,23,24].

4.1.2. Chloride binding in fly ash and LC^3 concretes

The Freundlich binding coefficients (k_b and m) obtained from the experiments and used in the simulations are shown in Table 3. The OPC concretes show higher chloride binding as noted from the coefficients k_b and m. These values are in the range of similar OPC concretes reported in [35,49,50]. The binding coefficients are slightly lower for the fly ash concretes, and the lowest for the LC^3 concretes. It needs to be noted that chloride binding is not just a function of the alumina content in the binder that enables the formation of chloroaluminates (Friedel's salt or Kuzel's salt). It also depends on the microstructure and alkalinity of the medium [49,50]. In general, an increase in fly ash content is found to increase the chloride binding capacity of concrete, attributable to the increased alumina content in fly ash [11,35,51]. However, the occurrence of C-S-H gel with reduced C/S ratios in mature fly ash concretes will lead to a reduction in the physically adsorbed chlorides on the gel surface [52]. Moreover, increased alkali contents in the pore solution can also hinder chloroaluminate formation [50]. Based on the chemical composition information from Table 1, Na_2O_{eq} for the OPC binder is 0.54% while it is 0.72% for the OPC-fly ash binder. The slightly lower chloride binding for the fly ash concrete could also be due to the low w/b [53,54] (0.35 as opposed to 0.45 for the OPC and LC^3 concretes) that results in a reduced fraction of fly ash having reacted.

It has been reported that the chloride binding capacity of LC^3

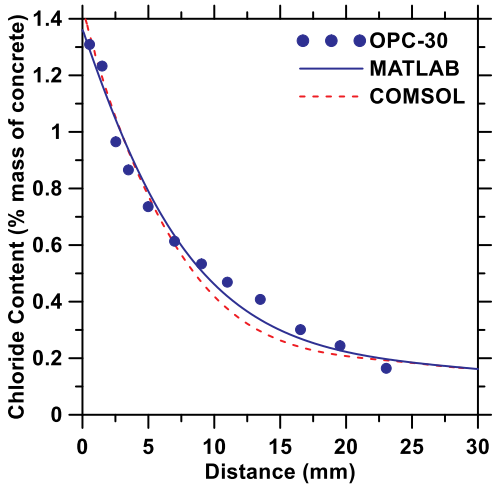

Fig. 2. Total chloride profiles predicted by the 1D and 2D models, and (b) free and bound Cl^- concentration distribution profiles from the 2D model after 56 days of simulation.

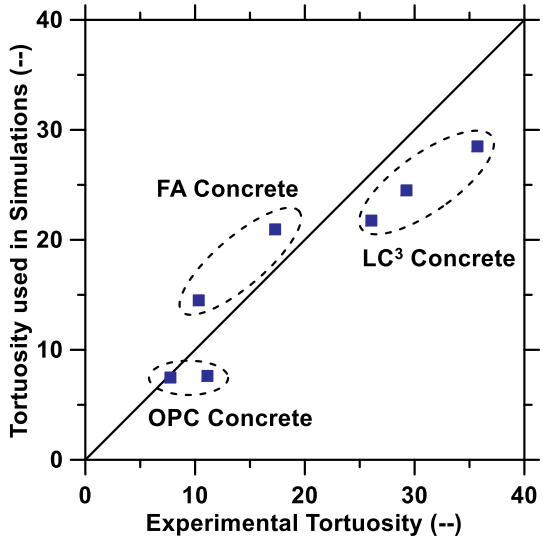

Fig. 3. Experimental tortuosities and those used for simulations.

binders is not higher than that of the OPC binders [23]. Studies have shown that the reduced chloride binding in limestone containing mixtures is not a consequence of dilution alone, rather, it is also due to the decreased ability of CO_3-AFm that replaces the SO_4-AFm in such mixtures to bind chlorides [50]. The chloride ions replace some carbonate ions from the mono- and hemi-carboaluminates formed in limestone-alumina bearing systems such as LC^3, forming a solid solution between CO_3-AFm and Cl-AFm [55]. Based on the above discussion, improved chloride transport processes for both the fly ash and LC^3 concretes can be mostly attributed to a dense and refined pore structure, even though the effect of chloride binding also needs to be accounted for, as is done here through Freundlich isotherms.

The simulated free and bound chloride concentrations in the pore solution at different depths after bulk diffusion experiments for 56 days are shown in Figs. 4 and 5 respectively. At any given depth beyond the first few mm, the LC^3 concretes have the lowest concentration of Cl^- in the pore solution, and the penetration rate is the slowest, dictated by the lower diffusion coefficients. For the high strength mixtures (B series), there is little difference between the free Cl^- concentration profiles of the fly ash and LC^3 concretes, even though the fly ash concrete was proportioned with a lower w/b. This points to the pore size refinement in the LC^3 concrete even at a higher w/b that results in significant retardation of transport. Also note that the LC^3 concrete demonstrated lower binding than the companion fly ash concrete as shown in Fig. 5. Comparing Fig. 5(a) and (b), it can be seen that the lower w/b mixtures demonstrate reduced Cl^- binding, which is in line with reported literature [56]. Another important observation from Figs. 4 and 5 is that, irrespective of the w/b used (in the range of 0.40 to 0.50), the difference in the free and bound chloride contents between different LC^3 mixtures is rather insignificant. At mature ages, the pozzolanic reactions and carboaluminate formation could have significantly progressed in all the LC^3 mixtures, thereby providing a similar microstructure for the mixtures with w/b in the chosen range. Data from a recent study has shown that LC^3 mixtures proportioned with w/b in the abovementioned range demonstrate similar mercury intrusion pore volumes and critical pore sizes as well as similar surface resistivity and rapid chloride permeability [24], corroborating these observations.

4.1.3. A parametric study of the effect of binding parameters

It is important to include the effect of Cl^- binding and the consequent reduction in pore solution Cl^- concentration in simulations of chloride transport to allow for accurate estimations of service life. However, binding parameters and the reaction rate constant used in the models are not always easy to estimate. Thus, it is important to understand the influence of these individual parameters on the transport simulation results. This study therefore evaluates the influence of k_b, m, and κ on the free chloride concentrations in the 30 MPa OPC concrete specimen (A series) subjected to 2800 mol/m^3 of external chlorides. The values of k_b and m obtained for this mixture from the experiments (9.29 and 0.34), and the value of κ used to obtain satisfactory fits in Fig. 1 (5×10^{-8}/s) are used as the baseline values. For the same k_b and κ, the influence of m on the free Cl^- profiles is significant only when the exponent approaches a value of 1.0 as observed in Fig. 6(a). The reported values of m generally lie between 0.1 and 0.6, and the profile changes are insignificant in this range when the other parameters remain the same. Fig. 6(b) shows the influence of k_b varying from 1 to 50 (the experimental value is 9.29) on the free Cl^- concentration profile. While an increase in k_b indicates increased binding that is represented by a drop in the free Cl^- concentration, the impact of changing k_b beyond a certain level is negligible. For example, simulations using k_b of 9.29 or 50 yield negligible changes in the concentration profiles. For a very low k_b of 1.0, the binding is significantly lower, and the free Cl^- concentrations are much higher, approaching that of the case where there is no binding. The influence of the reaction rate constant κ is shown in Fig. 6(c). This is a fitted parameter, as explained earlier. κ is varied from 1×10^{-6}/s to 1×10^{-9}/s in the simulations shown in Fig. 6(c). Within the range of values investigated, the rate constant is seen to have the highest impact on Cl^- transport. The lowest value of κ simulated, which is 1×10^{-9}/s can be considered as the limiting case where no binding occurs since the free Cl^- profile matches the one determined without the considering the effect of binding. For different mixtures used in this study, κ values that provided adequate fits the experimental data varied from 3×10^{-8}/s to 7×10^{-8}/s, which can be considered to be representative for typical concrete mixtures. As observed from previous work, values in the 10^{-6}/s range can be used for pastes, in the 10^{-7}/s range for mortars [42,43], and in the 10^{-8}/s range for concretes as found here.

4.2. Model predictions for long-term exposure

The 1D reaction-transport model is used to predict the response to long term exposure of chloride ions. The same concrete mixtures and the corresponding parameters listed in Tables 2 and 3 are used in the simulations. Fig. 7(a) and (b) show the total Cl^- concentration at a distance of 50 mm from the surface as a function of exposure duration; the former for a surface concentration (C_s) of 2800 mol/m^3 (used in the

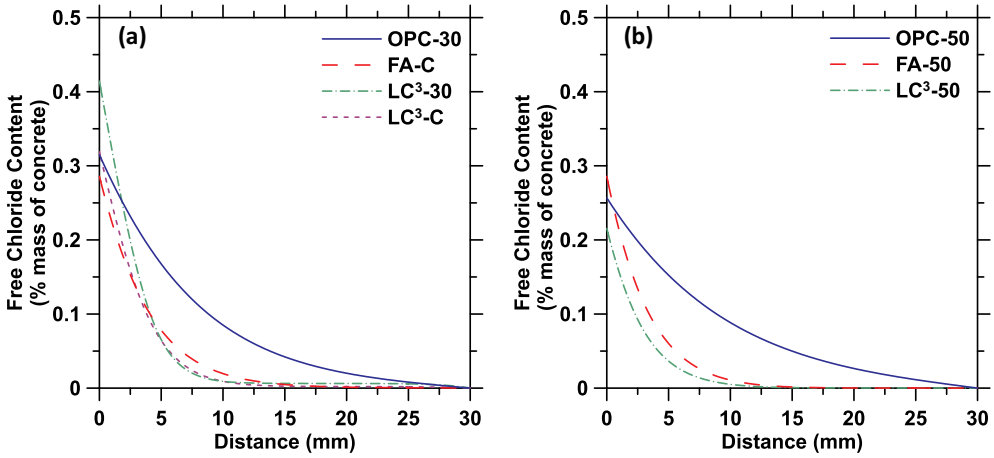

Fig. 4. Simulated free chloride concentrations as a function of depth for: (a) control and 30 MPa concretes (A series), and (b) 50 MPa concretes (B series).

bulk diffusion experiments), and the latter for a C_s of 870 mol/m^3 (corresponding to ~5% NaCl solution). As expected, a reduction in the surface concentration reduces the rate of ingress of chlorides. For the case where the surface concentration is lower (Fig. 7(b)), the simulations are carried out for 50 years. The mixtures with lower porosity and higher tortuosity, e.g., the LC^3 and low w/b fly ash concretes demonstrate slowly rising Cl^- concentrations at a depth of 50 mm as compared to the OPC concretes. Since the mixtures used in this study have differing w/b and mixture compositions which are known to influence the chloride threshold values (the concentration of Cl^- at the surface of steel to initiate corrosion) [57], a total Cl^- content by mass of concrete of 0.15–0.20% is used as the threshold to obtain a relative indication of the service life of these concretes [58].

For the surface Cl^- concentration corresponding to 5% NaCl (Fig. 7(b)), the OPC concretes exhibit corrosion initiation in < 5 years, while the LC^3 concretes take 30–35 years for corrosion initiation. Even if the corrosion threshold for the LC^3 concretes is considered to be lower than that of the OPC and fly ash concretes [26], and reduced binding effect as noted earlier accounted for, the significant enhancement in service-life can be ascribed to the lower diffusion coefficient of these mixtures, aided by the significant enhancement in tortuosity. Similar conclusions were also arrived at based on accelerated electrical transport and surface resistivity measurements [24]. This behavior can be explained by considering a simplified version of Eq. (9) without the reaction (binding) component; the porosity that is part of the left hand side and embedded in D_{eff} on the right hand side cancels each other, making the effective diffusion coefficient a function of the inverse square of tortuosity. Thus, even when there are minor differences in the overall pore volume (through which transport occurs), it is the tortuosity that dominates the rate of transport. As tortuosity is influenced by pore constrictivity also, it is then logical to conclude that refinement of transport-dominating pore sizes is more consequential in long term ionic transport, as evidenced by the high-performance systems. Fig. 7(c) shows the potential variability in chloride contents at a depth of 50 mm and consequently the time to corrosion initiation, based on the variabilities in the input parameters (Table 3) for the different Series B mixtures subjected to a 5% NaCl solution.

4.3. Incorporating damage in transport simulations: Relative service-life projections

The foregoing discussions on ionic transport were limited to pristine, undamaged concretes, as is generally implemented in many service-life models. Cracking is a common occurrence in reinforced concrete that can significantly impact its service life. For example, it is reported that in cracked regions of bridge decks, chloride levels required to initiate corrosion can be reached as early as 1 year [59]. Several studies have examined the influence of loading and cracking on chloride transport and reinforcement corrosion [60–62]. The effect of crack width, density, location and tortuosity on chloride diffusion [63–67], considerations of a damage zone with properties different than those of the bulk [68], and crack propagation coupled with diffusion [69] have been studied using numerical models. Generally, 2D models are used for simulations of transport in cracked concretes since

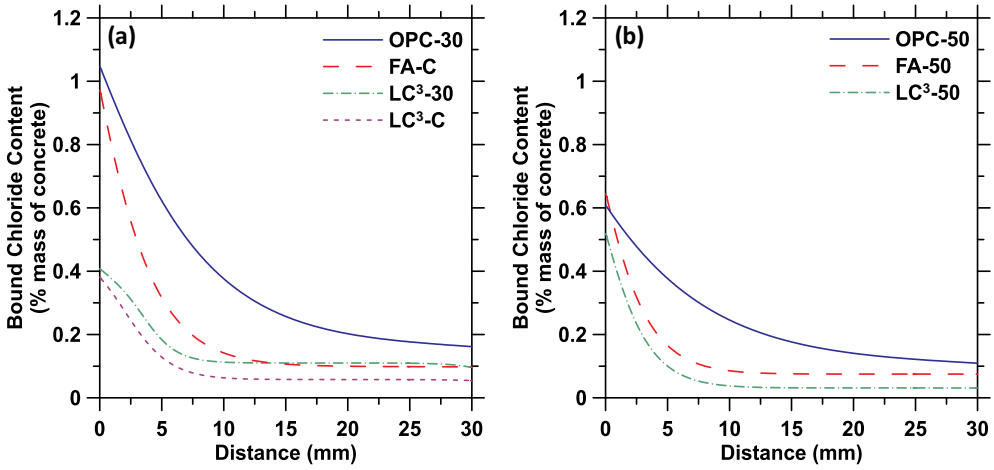

Fig. 5. Simulated bound chloride concentrations as a function of depth for: (a) control and 30 MPa concretes (A series), and (b) 50 MPa concretes (B series).

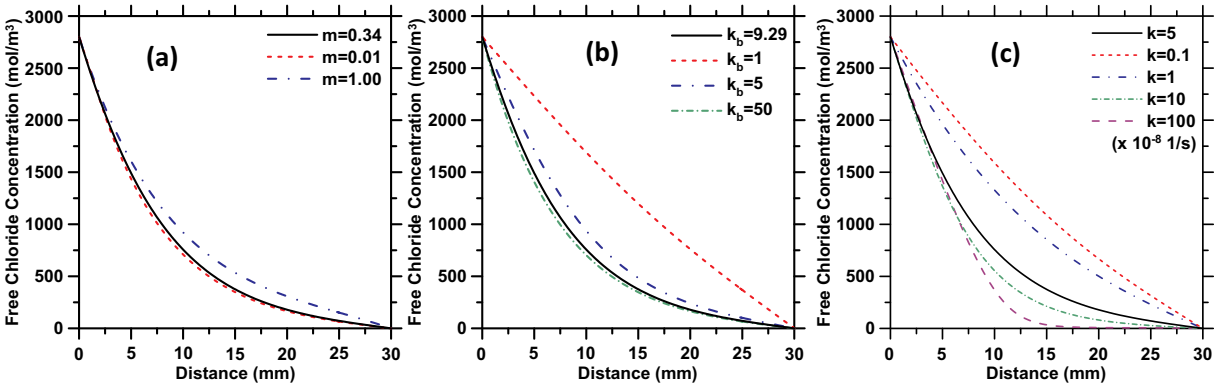

Fig. 6. Parametric investigations on the effect of binding parameters: (a) varying m, (b) varying k_b, and (c) varying κ.

the crack width and depth need to be considered in the analysis.

4.3.1. Damage parameter

This paper incorporates the effect of damage due to repeated loading (fatigue) into the transport model. Fatigue loading results in initiation and growth of microcracks in concrete. Rather than accounting for discrete cracks and simulating the concomitant magnification in transport [43,69–71], the damage due to fatigue loading is considered here to be uniform such that the effective diffusion coefficient of Cl^- in the damaged concrete (D_{eff}^d) is influenced by the damage parameter (d) as shown in Eq. (12). No attempt is made to distinguish between the tensile and compressive zones under flexural fatigue which

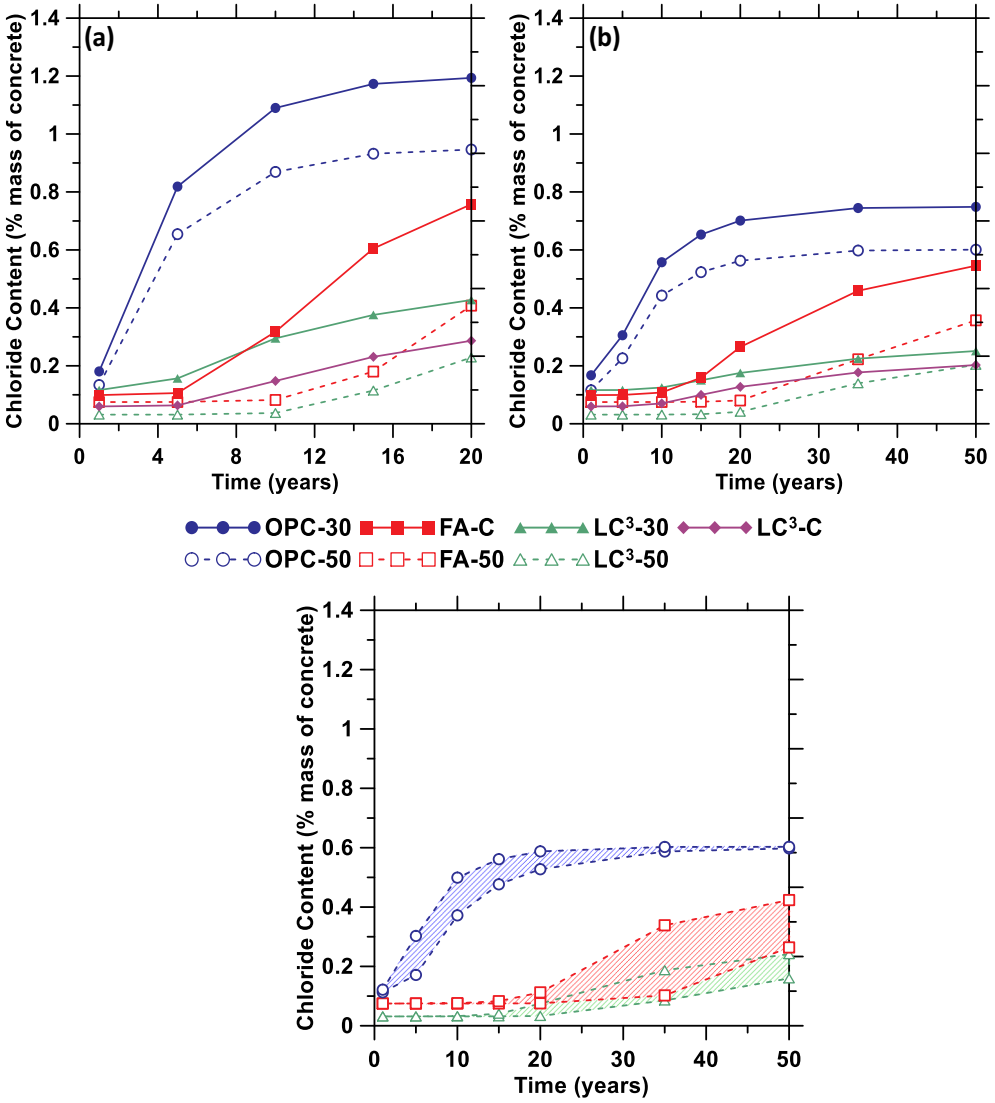

Fig. 7. Total chloride contents at a distance of 50 mm from the surface, as a function of exposure time: (a) C_s of 2800 mol/m^3, (b) C_s of 870 mol/m^3, (c) variability in chloride contents considering the variability in experimental measurements for the series B mixtures subjected to C_s of 870 mol/m^3.

could have differing degrees of damage [72]. The damage parameter is simply defined as the ratio of number of load cycles at a certain time (n) to the number of cycles to failure (N_f), according to Miner's rule as shown in Eq. (13) [73]. The number of load cycles can be determined from the frequency of loading (f) and time (t) [74]. The randomness of the distribution of microcracks under cyclic loading can be assumed to result in an isotropic discontinuous state [75], which can be modeled using a scalar continuous damage variable. Thus, the simulations can be carried out in a 1D space also since the discontinuous state is represented by a continuous variable.

$$D_{eff}^{d} = D_{eff}\frac{1}{(1-d)^2} \tag{12}$$

$$d = \frac{n}{N_f} = \frac{ft}{N_f} \tag{13}$$

Stress-number of cycles (S—N) curves are commonly employed to determine fatigue lives of concrete under different stress levels. The S—N curve of concrete can be represented as shown below [76]:

$$S = a - b(\log N_f) \tag{14}$$

The fitting coefficients a and b for flexural fatigue have been reported to be approximately 1.05–1.15 and 0.07–0.11 respectively for a number of normal weight and lightweight concretes with different compositions with or without fiber reinforcement [77–79]. In this study, a and b are taken as 1.07 and 0.09 respectively for all the mixtures. From Eqs. (13) and (14), the damage parameter can be represented as a function of time as:

$$d = \frac{ft}{10^{(a-S)/b}} \tag{15}$$

Since damage parameter is a function of time, the diffusion coefficient in this formulation is also time-dependent (in addition to its concentration-dependence, which is also a function of time). D_{eff}^{d} from Eq. (12) is used in Eq. (9) and solved using the 1D simulation model to develop the chloride concentration profiles. The same formulation is also used in a 2D framework in COMSOL.

Fig. 8 shows the free Cl^- concentration profile of the 50 MPa concretes (B series) in both the undamaged condition as well as when a stress level (S) of 0.60 is applied for a duration of 56 days after 1 year of moist curing. The free Cl^- concentration at any depth is higher for the damaged case, as expected. The effect of damage is more pronounced for the OPC concrete as compared to the fly ash and LC^3 concretes

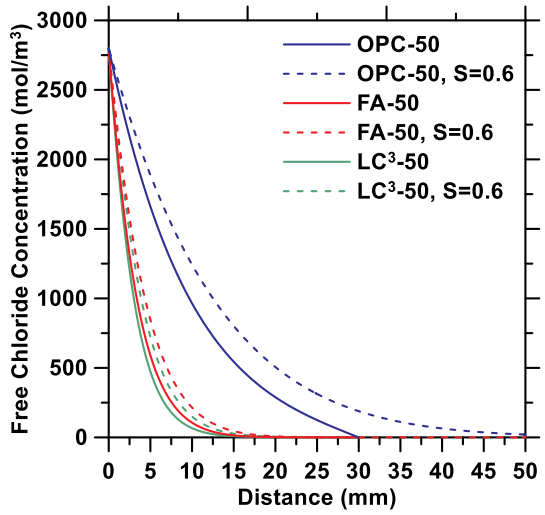

Fig. 8. Free Cl^- concentration profiles of the 50 MPa concretes (B series) – undamaged and subjected to a stress level (S) of 0.60, after 56 days of natural diffusion (C_s = 2800 mol/m^3).

because of the higher effective diffusion coefficients in the undamaged state. When the same duration of stress application is considered, along with the same parameters of the S—N curve (a and b) and the same frequency of loading, the damage parameter is invariant of the mixture composition. It needs to be noted that, in the absence of experimental data on the fatigue performance of modified concretes, the parameters a and b are assumed to be invariant of the mixture type (which is a reasonable assumption, based on [77,79,80]), and hence the level of damage is only dependent on the duration of loading and exposure. Lower initial effective diffusion coefficients of fly ash and LC^3 concretes result in a less significant effect of damage on the chloride profiles as can be observed from Fig. 8. Fig. 9 shows the COMSOL simulations (50 mm depth) for 180 days showing the free Cl^- concentrations. The enhancement in transport because of damage is much higher for the OPC concrete as evidenced in these figures, because of reasons described earlier.

4.3.2. Relative service-life estimations

Estimations of relative time to corrosion initiation are carried out for the 50 MPa OPC, fly ash, and LC^3 concretes (B series mixtures) in the undamaged condition as well as when subjected to stress levels (S) of 0.3, 0.4, and 0.5, under surface concentrations of 870 mol/m^3 (~5% NaCl solution). 1D simulations were carried out using the appropriate parameters shown in Table 3. The effective diffusion coefficients of these mixtures determined using Eq. (11) were modified by the damage parameter corresponding to the duration of simulation as determined from Eq. (15).

For the undamaged condition and for S of 0.3, simulations were carried out for a duration of 150 years, while the simulation duration was reduced to 75 years for S of 0.4 and 6 years for S of 0.5. This is on account of the fact that at higher stress levels, failure is reached in fewer number of cycles, i.e., at lower times. Since the aim is to examine the influence of damage on service life as well as the relative performance of the three mixtures, the time to corrosion initiation relative to that of the undamaged concrete is obtained through normalizing by 150 years. The simulations were stopped when the ratio of Cl^- concentration at the rebar (which is at 50 mm from the surface) to that at the surface (C_s = 870 mol/m^3) reached ~0.50 since, for most types of reinforcements, corrosion is expected to initiate before this value of C_{steel}/C_s. It has been reported that for uncoated steel and concrete containing no corrosion inhibitor, C_{steel}/C_s can be taken as 0.1, while it can be increased to 0.3 if a corrosion inhibitor is used and 0.5 for epoxy coated steel reinforcement [81]. The effects of the physical presence of rebar that increases the local Cl^- concentration is not considered here.

Fig. 10 (a)-(c) depict the relative time to corrosion initiation for the three different concretes at different C_{steel}/C_s values. While the simulations were carried out for 150 years for the undamaged concretes, the higher diffusion coefficient in the OPC mixture resulted in a C_{steel}/C_s value close to 0.5 at an age of 50 years; in other words, to attain this C_{steel}/C_s required only a third of the time for the OPC concretes. This can be easily noticed in the comparison between Fig. 10(a) and Fig. 10(b) and (c). In all the three cases, it can be seen that a stress level of 0.3 induces only minor damage, and the transport process is not significantly affected. For the undamaged case and at S of 0.3, considering the C_{steel}/C_s for corrosion initiation to be equal to 0.2 (0.1 to 0.3 for typical field exposures [43]), the service life is between 12 and 14 years for the OPC concrete, between 70 and 75 years for the fly ash concrete, and 65 and 70 years for the LC^3 concrete, in line with the trends in [26] for similar mixtures. If the reduction in Cl^- threshold for the modified binders are considered, their service lives drop by around 10%. Realistic Cl^- threshold values can be used along with the simulation output shown here to determine accurate service lives.

When the stress level is increased to 0.4, a significant drop in service life ensues. The time to corrosion initiation drops to 10, 42, and 39 years respectively for the OPC, fly ash, and LC^3 concretes. The number of cycles to failure at this stress level translates to a life of

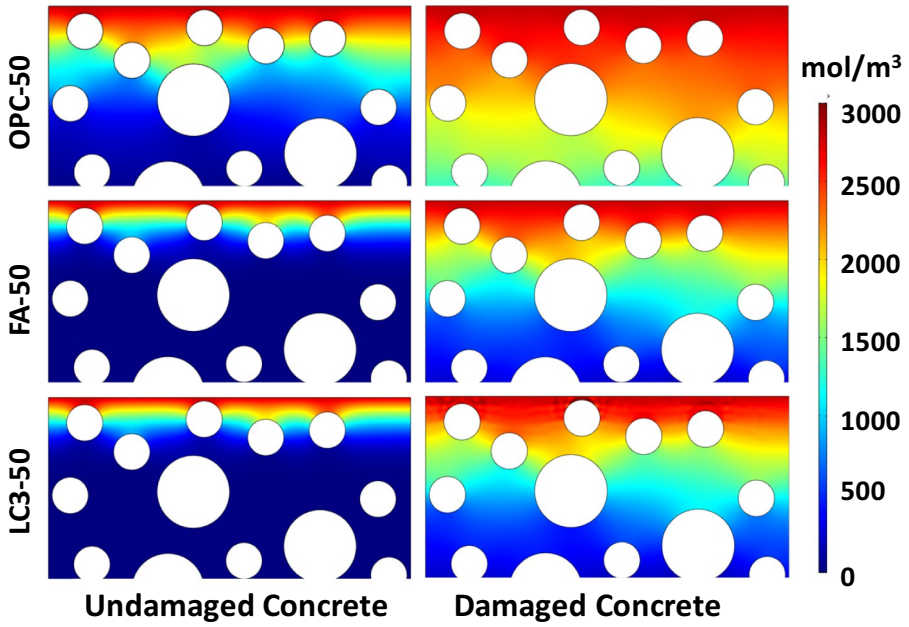

Fig. 9. Free Cl^- concentration simulated using COMSOL for the 50 MPa concretes (B series) - undamaged and subjected to a stress level (S) of 0.60, after 180 days of natural diffusion (C_s = 2800 mol/m^3). Only a 50 mm depth is shown here.

~75 years, and hence the maximum time for corrosion initiation relative to the undamaged concrete is 50% at a C_{steel}/C_s of about 0.46. Similarly, load-induced end of life is about 6 years for a stress level of 0.5. In this case, for the fly ash and LC^3 concretes, the simulations are ended at a C_{steel}/C_s of around 0.2 since that is the maximum level of relative concentration experienced at 50 mm in this duration. For OPC concrete, a higher diffusion coefficient results in a C_{steel}/C_s of around 0.45 for the same duration. High levels of damage (e.g., S = 0.5) result in similar service life between the different concrete mixtures as can be noted from these figures. This is because at higher values of d, the diffusion coefficients in the damaged condition (D_{eff}^d) predicted by Eq. (12) are very high for all the concretes. High levels of microcracking and damage have been reported to reduce the difference between transport properties of normal and high-performance concretes [82], as observed in these figures.

5. Conclusions

Numerical simulation of diffusion was carried out through explicit considerations of the tortuosity of the pore network, concentration-dependence of the diffusion coefficients, and chloride binding. Concretes proportioned using a limestone-calcined clay cement (LC^3) and those containing fly ash were used to demonstrate the applicability of the model.

An effective diffusion coefficient obtained from considerations of pore geometry was modified with concentration-dependence using equivalent conductivities. The pore tortuosity and the Fruendlich isotherm parameters for chloride binding were obtained from experimental data while the binding rate constant was obtained through fitting the model to the experimental data. Within a range of commonly reported Freundlich binding parameters for concretes, their influence on free Cl^- concentrations were estimated using a parametric study. Using the input values ascertained from simulations of the bulk diffusion test, the model was used to simulate the long-term transport performance of the LC^3, fly ash, and control concrete mixtures. While LC^3 and fly ash concretes exhibited similar pore volumes and reduced binding as compared to the control concrete, the total chloride concentrations at the level of the reinforcing steel were significantly lower, demonstrating the beneficial effects of improved tortuosity of the pore network. The LC^3 concretes had the highest pore tortuosities even at slightly higher w/b than fly ash concretes, showing the amplification of pore refinement in such mixtures that leads to better transport properties.

In an effort to simulate transport conditions under damage, the

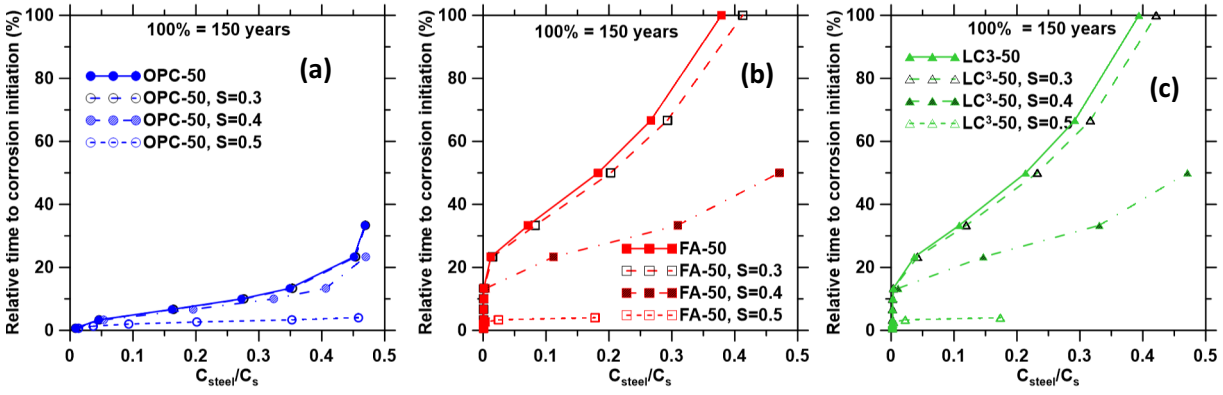

Fig. 10. Projected service lives in the undamaged and damaged (S = 0.3, 0.4, 0.5) conditions for the 50 MPa (B series) mixtures: (a) OPC concrete, (b) fly ash concrete, and (c) LC^3 concrete.

chloride transport model was augmented by an isotropic damage parameter that represents the discontinuous microscopic damage state. The damage variable under different imposed stress levels was derived from S−N relationships under fatigue. The time to corrosion initiation when subjected to 5% NaCl solution was determined as a function of the ratio of free Cl^- concentration at the level of the reinforcing steel to that at the surface, under different stress levels. The durability enhancement of the LC^3 and fly ash concretes at lower stress levels, and the relative invariance of service life under higher stress levels were brought out. The proposed modeling approach can be used to evaluate the influence of binder composition and damage on effective service-life of chloride-exposed concrete structures, and as a methodology for high-performance binder selection. The pore structure features (porosity and tortuosity) and binding parameters, which are functions of the mixture composition, are the required model inputs for transport and service-life prediction. A priori knowledge of these parameters (as used here), or their estimates based on mixture composition and exposure age can be used for predictive purposes or binder selection.

Credit author statement

Pu Yang: Methodology, Validation, Investigation, Writing-Original Draft, Formal analysis, Visualization.

Yuvaraj Dhandapani: Investigation, Resources, Data Curation.

Manu Santhanam: Resources, Writing-Editing and Review.

Narayanan Neithalath: Conceptualization, Methodology, Writing-Editing and Review, Supervision, Project administration.

Declaration of competing interest

The authors declare that they have no known competing financial interests or personal relationships that could have appeared to influence the work reported in this paper.

Acknowledgments

The experimental work reported in this paper was carried out in the concrete laboratory at IIT Madras while the simulations were carried out in the computational mechanics laboratory at Arizona State University. Partial financial support from the Swiss Agency for Development and Cooperation (SDC) (Project number: 7F-08527.02.01) for the experimental study carried out as a part of LC^3 project Phase-1 is gratefully acknowledged. The corresponding author acknowledges the VAJRA faculty fellowship of the Science and Engineering Research Board of the Government of India.

References

[1] Nace-International-Report.pdf, (n.d.). http://impact.nace.org/documents/Nace-International-Report.pdf (accessed April 18, 2019).
[2] L. Tang, Concentration dependence of diffusion and migration of chloride ions: part 1. Theoretical considerations, Cem. Concr. Res. 29 (1999) 1463–1468, https://doi.org/10.1016/S0008-8846(99)00121-0.
[3] E. Samson, J. Marchand, J.-L. Robert, J.-P. Bournazel, Modelling ion diffusion mechanisms in porous media, Int. J. Numer. Methods Eng. 46 (1999) 2043–2060, https://doi.org/10.1002/(SICI)1097-0207(19991230)46:12<2043::AID-NME795>3.0.CO;2-7.
[4] P. Spiesz, H.J.H. Brouwers, The apparent and effective chloride migration coefficients obtained in migration tests, Cem. Concr. Res. 48 (2013) 116–127, https://doi.org/10.1016/j.cemconres.2013.02.005.
[5] P. Yang, G. Sant, N. Neithalath, A refined, self-consistent Poisson-Nernst-Planck (PNP) model for electrically induced transport of multiple ionic species through concrete, Cem. Concr. Compos. 82 (2017) 80–94, https://doi.org/10.1016/j.cemconcomp.2017.05.015.
[6] K. Krabbenhøft, J. Krabbenhøft, Application of the Poisson–Nernst–Planck equations to the migration test, Cem. Concr. Res. 38 (2008) 77–88, https://doi.org/10.1016/j.cemconres.2007.08.006.
[7] C. Andrade, M.A. Sanjuán, A. Recuero, O. Río, Calculation of chloride diffusivity in concrete from migration experiments, in non-steady-state conditions, Cem. Concr. Res. 24 (1994) 1214–1228, https://doi.org/10.1016/0008-8846(94)90106-6.
[8] E. Samson, J. Marchand, K.A. Snyder, Calculation of ionic diffusion coefficients on the basis of migration test results, Mater. Struct. 36 (2003) 156–165, https://doi.org/10.1007/BF02479554.
[9] X. Shi, N. Xie, K. Fortune, J. Gong, Durability of steel reinforced concrete in chloride environments: an overview, Constr. Build. Mater. 30 (2012) 125–138, https://doi.org/10.1016/j.conbuildmat.2011.12.038.
[10] Y. Wang, Z. Shui, X. Gao, R. Yu, Y. Huang, S. Cheng, Understanding the chloride binding and diffusion behaviors of marine concrete based on Portland limestone cement-alumina enriched pozzolans, Constr. Build. Mater. 198 (2019) 207–217, https://doi.org/10.1016/j.conbuildmat.2018.11.270.
[11] T. Cheewaket, C. Jaturapitakkul, W. Chalee, Long term performance of chloride binding capacity in fly ash concrete in a marine environment, Constr. Build. Mater. 24 (2010) 1352–1357, https://doi.org/10.1016/j.conbuildmat.2009.12.039.
[12] M. Gbozee, K. Zheng, F. He, X. Zeng, The influence of aluminum from metakaolin on chemical binding of chloride ions in hydrated cement pastes, Appl. Clay Sci. 158 (2018) 186–194, https://doi.org/10.1016/j.clay.2018.03.038.
[13] Z. Shi, M.R. Geiker, K. De Weerdt, T.A. Østnor, B. Lothenbach, F. Winnefeld, J. Skibsted, Role of calcium on chloride binding in hydrated Portland cement–metakaolin–limestone blends, Cem. Concr. Res. 95 (2017) 205–216, https://doi.org/10.1016/j.cemconres.2017.02.003.
[14] C. Qiao, P. Suraneni, T. Nathalene Wei Ying, A. Choudhary, J. Weiss, Chloride binding of cement pastes with fly ash exposed to CaCl2 solutions at 5 and 23 °C, Cem. Concr. Compos. 97 (2019) 43–53, https://doi.org/10.1016/j.cemconcomp.2018.12.011.
[15] M. Antoni, J. Rossen, F. Martirena, K. Scrivener, Cement substitution by a combination of metakaolin and limestone, Cem. Concr. Res. 42 (2012) 1579–1589, https://doi.org/10.1016/j.cemconres.2012.09.006.
[16] K. De Weerdt, K.O. Kjellsen, E. Sellevold, H. Justnes, Synergy between fly ash and limestone powder in ternary cements, Cem. Concr. Compos. 33 (2011) 30–38, https://doi.org/10.1016/j.cemconcomp.2010.09.006.
[17] K. De Weerdt, M.B. Haha, G. Le Saout, K.O. Kjellsen, H. Justnes, B. Lothenbach, Hydration mechanisms of ternary Portland cements containing limestone powder and fly ash, Cem. Concr. Res. 41 (2011) 279–291, https://doi.org/10.1016/j.cemconres.2010.11.014.
[18] M. Aguayo, P. Yang, K. Vance, G. Sant, N. Neithalath, Electrically driven chloride ion transport in blended binder concretes: insights from experiments and numerical simulations, Cem. Concr. Res. 66 (2014) 1–10, https://doi.org/10.1016/j.cemconres.2014.07.022.
[19] G. Puerta-Falla, M. Balonis, G.L. Saout, G. Falzone, C. Zhang, N. Neithalath, G. Sant, Elucidating the role of the aluminous source on limestone reactivity in cementitious materials, J. Am. Ceram. Soc. 98 (2015) 4076–4089, https://doi.org/10.1111/jace.13806.
[20] K. Vance, M. Aguayo, T. Oey, G. Sant, N. Neithalath, Hydration and strength development in ternary portland cement blends containing limestone and fly ash or metakaolin, Cem. Concr. Compos. 39 (2013) 93–103, https://doi.org/10.1016/j.cemconcomp.2013.03.028.
[21] A. Arora, G. Sant, N. Neithalath, Ternary blends containing slag and interground/blended limestone: hydration, strength, and pore structure, Constr. Build. Mater. 102 (2016) 113–124, https://doi.org/10.1016/j.conbuildmat.2015.10.179.
[22] D.P. Bentz, C.F. Ferraris, K.A. Snyder, Best Practices Guide for High-volume Fly Ash Concretes : Assuring Properties and Performance, National Institute of Standards and Technology, 2013, https://doi.org/10.6028/NIST.TN.1812.
[23] K. Scrivener, F. Martirena, S. Bishnoi, S. Maity, Calcined clay limestone cements (LC3), Cem. Concr. Res. 114 (2018) 49–56, https://doi.org/10.1016/j.cemconres.2017.08.017.
[24] Y. Dhandapani, T. Sakthivel, M. Santhanam, R. Gettu, R.G. Pillai, Mechanical properties and durability performance of concretes with limestone calcined clay cement (LC3), Cem. Concr. Res. 107 (2018) 136–151, https://doi.org/10.1016/j.cemconres.2018.02.005.
[25] Y. Dhandapani, M. Santhanam, Assessment of pore structure evolution in the limestone calcined clay cementitious system and its implications for performance, Cem. Concr. Compos. 84 (2017) 36–47, https://doi.org/10.1016/j.cemconcomp.2017.08.012.
[26] R.G. Pillai, R. Gettu, M. Santhanam, S. Rengaraju, Y. Dhandapani, S. Rathnarajan, A.S. Basavaraj, Service life and life cycle assessment of reinforced concrete systems with limestone calcined clay cement (LC3), Cem. Concr. Res. 118 (2019) 111–119, https://doi.org/10.1016/j.cemconres.2018.11.019.
[27] A. Atkinson, A.K. Nickerson, The diffusion of ions through water-saturated cement, J. Mater. Sci. 19 (1984) 3068–3078.
[28] L. Shen, Z. Chen, Critical review of the impact of tortuosity on diffusion, Chem. Eng. Sci. 62 (2007) 3748–3755, https://doi.org/10.1016/j.ces.2007.03.041.
[29] D.C. Herrick, W.D. Kennedy, Electrical efficiency—a pore geometric theory for interpreting the electrical properties of reservoir rocks, GEOPHYSICS 59 (1994) 918–927, https://doi.org/10.1190/1.1443651.
[30] N. Neithalath, J. Jain, Relating rapid chloride transport parameters of concretes to microstructural features extracted from electrical impedance, Cem. Concr. Res. 40 (2010) 1041–1051, https://doi.org/10.1016/j.cemconres.2010.02.016.
[31] D. Trejo, M. Shakouri, N.P. Vaddey, O.B. Isgor, Development of empirical models for chloride binding in cementitious systems containing admixed chlorides, Constr. Build. Mater. 189 (2018) 157–169, https://doi.org/10.1016/j.conbuildmat.2018.08.197.
[32] B. Martín-Pérez, H. Zibara, R.D. Hooton, M.D.A. Thomas, A study of the effect of chloride binding on service life predictions, Cem. Concr. Res. 30 (2000) 1215–1223. doi:https://doi.org/10.1016/S0008-8846(00)00339-2.
[33] T. Luping, L.-O. Nilsson, Chloride binding capacity and binding isotherms of OPC pastes and mortars, Cem. Concr. Res. 23 (1993) 247–253, https://doi.org/10.1016/0008-8846(93)90089-R.

[34] J. Li, W. Shao, The effect of chloride binding on the predicted service life of RC pipe piles exposed to marine environments, Ocean Eng. 88 (2014) 55–62, https://doi.org/10.1016/j.oceaneng.2014.06.021.

[35] M.D.A. Thomas, R.D. Hooton, A. Scott, H. Zibara, The effect of supplementary cementitious materials on chloride binding in hardened cement paste, Cem. Concr. Res. 42 (2012) 1–7, https://doi.org/10.1016/j.cemconres.2011.01.001.

[36] Q. Yuan, C. Shi, G. De Schutter, K. Audenaert, D. Deng, Chloride binding of cement-based materials subjected to external chloride environment – a review, Constr. Build. Mater. 23 (2009) 1–13, https://doi.org/10.1016/j.conbuildmat.2008.02.004.

[37] A. Vollpracht, B. Lothenbach, R. Snellings, J. Haufe, The pore solution of blended cements: a review, Mater. Struct. 49 (2016) 3341–3367, https://doi.org/10.1617/s11527-015-0724-1.

[38] R.S. Barneyback, S. Diamond, Expression and analysis of pore fluids from hardened cement pastes and mortars, Cem. Concr. Res. 11 (1981) 279–285, https://doi.org/10.1016/0008-8846(81)90069-7.

[39] J. Allen, Estimation of Pore Solution Conductivity, NIST, 2017, https://www.nist.gov/el/materials-and-structural-systems-division-73100/inorganic-materials-group-73103/estimation-pore , Accessed date: 19 April 2019.

[40] K.A. Snyder, X. Feng, B.D. Keen, T.O. Mason, Estimating the electrical conductivity of cement paste pore solutions from OH−, K+ and Na+ concentrations, Cem. Concr. Res. 33 (2003) 793–798, https://doi.org/10.1016/S0008-8846(02)01068-2.

[41] A.C. Emmanuel, P. Haldar, S. Maity, S. Bishnoi, Second pilot production of limestone calcined clay cement in India: the experience, Indian Concr J 90 (2016) 57–64.

[42] P. Spiesz, M.M. Ballari, H.J.H. Brouwers, RCM: a new model accounting for the non-linear chloride binding isotherm and the non-equilibrium conditions between the free- and bound-chloride concentrations, Constr. Build. Mater. 27 (2012) 293–304, https://doi.org/10.1016/j.conbuildmat.2011.07.045.

[43] D.P. Bentz, E.J. Garboczi, Y. Lu, N. Martys, A.R. Sakulich, W.J. Weiss, Modeling of the influence of transverse cracking on chloride penetration into concrete, Cem. Concr. Compos. 38 (2013) 65–74, https://doi.org/10.1016/j.cemconcomp.2013.03.003.

[44] Y. Wang, L. Wu, Y. Wang, Q. Li, Z. Xiao, Prediction model of long-term chloride diffusion into plain concrete considering the effect of the heterogeneity of materials exposed to marine tidal zone, Constr. Build. Mater. 159 (2018) 297–315, https://doi.org/10.1016/j.conbuildmat.2017.10.083.

[45] Y. Tian, Z. Tian, N. Jin, X. Jin, W. Yu, A multiphase numerical simulation of chloride ions diffusion in concrete using electron microprobe analysis for characterizing properties of ITZ, Constr. Build. Mater. 178 (2018) 432–444, https://doi.org/10.1016/j.conbuildmat.2018.05.047.

[46] N. Benkemoun, M.N. Hammood, O. Amiri, Embedded finite element formulation for the modeling of chloride diffusion accounting for chloride binding in meso-scale concrete, Finite Elem. Anal. Des. 130 (2017) 12–26, https://doi.org/10.1016/j.finel.2017.03.003.

[47] M.B. Clennell, Tortuosity: a guide through the maze, Dev. Petrophysics (1997) 299–344.

[48] C.J. Gommes, A.-J. Bons, S. Blacher, J.H. Dunsmuir, A.H. Tsou, Practical methods for measuring the tortuosity of porous materials from binary or gray-tone tomographic reconstructions, AICHE J. 55 (2009) 2000–2012, https://doi.org/10.1002/aic.11812.

[49] Z. Yang, Y. Gao, S. Mu, H. Chang, W. Sun, J. Jiang, Improving the chloride binding capacity of cement paste by adding nano-Al2O3, Constr. Build. Mater. 195 (2019) 415–422, https://doi.org/10.1016/j.conbuildmat.2018.11.012.

[50] A. Ipavec, T. Vuk, R. Gabrovšek, V. Kaučič, Chloride binding into hydrated blended cements: the influence of limestone and alkalinity, Cem. Concr. Res. 48 (2013) 74–85.

[51] E.G. Moffatt, M.D.A. Thomas, A. Fahim, Performance of high-volume fly ash concrete in marine environment, Cem. Concr. Res. 102 (2017) 127–135, https://doi.org/10.1016/j.cemconres.2017.09.008.

[52] J.J. Beaudoin, V.S. Ramachandran, R.F. Feldman, Interaction of chloride and C-S-H, Cem. Concr. Res. 20 (1990) 875–883, https://doi.org/10.1016/0008-8846(90)90049-4.

[53] H. Zibara, National Library of Canada= Bibliothèque nationale du Canada (Ed.), Binding of External Chlorides by Cement Pastes, 2001 PhD Thesis.

[54] R. Loser, B. Lothenbach, A. Leemann, M. Tuchschmid, Chloride resistance of concrete and its binding capacity – comparison between experimental results and thermodynamic modeling, Cem. Concr. Compos. 32 (2010) 34–42, https://doi.org/10.1016/j.cemconcomp.2009.08.001.

[55] M. Balonis, B. Lothenbach, G. Le Saout, F.P. Glasser, Impact of chloride on the mineralogy of hydrated Portland cement systems, Cem. Concr. Res. 40 (2010) 1009–1022.

[56] J. Liu, G. Ou, Q. Qiu, X. Chen, J. Hong, F. Xing, Chloride transport and microstructure of concrete with/without fly ash under atmospheric chloride condition, Constr. Build. Mater. 146 (2017) 493–501, https://doi.org/10.1016/j.conbuildmat.2017.04.018.

[57] F. Pargar, D.A. Koleva, K. van Breugel, Determination of chloride content in Cementitious materials: from fundamental aspects to application of Ag/AgCl chloride sensors, Sensors 17 (2017), https://doi.org/10.3390/s17112482.

[58] U. Angst, B. Elsener, C.K. Larsen, Ø. Vennesland, Critical chloride content in reinforced concrete — a review, Cem. Concr. Res. 39 (2009) 1122–1138, https://doi.org/10.1016/j.cemconres.2009.08.006.

[59] W.D. Lindquist, D. Darwin, J. Browning, G.G. Miller, Effect of Cracking on Chloride Content in Concrete Bridge Decks, American Concrete Institute, 2006.

[60] J. Wang, P.A.M. Basheer, S.V. Nanukuttan, A.E. Long, Y. Bai, Influence of service loading and the resulting micro-cracks on chloride resistance of concrete, Constr. Build. Mater. 108 (2016) 56–66, https://doi.org/10.1016/j.conbuildmat.2016.01.005.

[61] S. Jones, N. Martys, Y. Lu, D. Bentz, Simulation studies of methods to delay corrosion and increase service life for cracked concrete exposed to chlorides, Cem. Concr. Compos. 58 (2015) 59–69, https://doi.org/10.1016/j.cemconcomp.2014.12.014.

[62] J. Xu, F. Li, J. Zhao, L. Huang, Model of time-dependent and stress-dependent chloride penetration of concrete under sustained axial pressure in the marine environment, Constr. Build. Mater. 170 (2018) 207–216, https://doi.org/10.1016/j.conbuildmat.2018.03.077.

[63] T. Ishida, P.O. Iqbal, H.T.L. Anh, Modeling of chloride diffusivity coupled with non-linear binding capacity in sound and cracked concrete, Cem. Concr. Res. 39 (2009) 913–923.

[64] H.-L. Wang, J.-G. Dai, X.-Y. Sun, X.-L. Zhang, Characteristics of concrete cracks and their influence on chloride penetration, Constr. Build. Mater. 107 (2016) 216–225, https://doi.org/10.1016/j.conbuildmat.2016.01.002.

[65] S.Y. Jang, B.S. Kim, B.H. Oh, Effect of crack width on chloride diffusion coefficients of concrete by steady-state migration tests, Cem. Concr. Res. 41 (2011) 9–19.

[66] S.-S. Park, S.-J. Kwon, S.H. Jung, Analysis technique for chloride penetration in cracked concrete using equivalent diffusion and permeation, Constr. Build. Mater. 29 (2012) 183–192.

[67] Q. Liu, J. Yang, J. Xia, D. Easterbrook, L. Li, X.-Y. Lu, A numerical study on chloride migration in cracked concrete using multi-component ionic transport models, Comput. Mater. Sci. 99 (2015) 396–416, https://doi.org/10.1016/j.commatsci.2015.01.013.

[68] J. Peng, S. Hu, J. Zhang, C.S. Cai, L. Li, Influence of cracks on chloride diffusivity in concrete: a five-phase mesoscale model approach, Constr. Build. Mater. 197 (2019) 587–596, https://doi.org/10.1016/j.conbuildmat.2018.11.208.

[69] M. Kurumatani, H. Anzo, K. Kobayashi, S. Okazaki, S. Hirose, Damage model for simulating chloride concentration in reinforced concrete with internal cracks, Cem. Concr. Compos. 84 (2017) 62–73, https://doi.org/10.1016/j.cemconcomp.2017.08.015.

[70] J. Weiss, J. Couch, B. Pease, P. Laugesen, M. Geiker, Influence of mechanically induced cracking on chloride ingress in concrete, J. Mater. Civ. Eng. 29 (2017) 04017128, , https://doi.org/10.1061/(ASCE)MT.1943-5533.0001922.

[71] C. Gu, G. Ye, W. Sun, A review of the chloride transport properties of cracked concrete: experiments and simulations, J. Zhejiang Univ.-Sci. A. 16 (2015) 81–92, https://doi.org/10.1631/jzus.A1400247.

[72] J. Wu, B. Diao, W. Zhang, Y. Ye, Z. Liu, D. Wang, Chloride diffusivity and service life prediction of fatigue damaged RC beams under seawater wet-dry environment, Constr. Build. Mater. 171 (2018) 942–949, https://doi.org/10.1016/j.conbuildmat.2018.03.145.

[73] J. Lemaitre, J. Dufailly, Damage measurements, Eng. Fract. Mech. 28 (1987) 643–661, https://doi.org/10.1016/0013-7944(87)90059-2.

[74] B. Guan, J. Wu, T. Yang, A. Xu, Y. Sheng, H. Chen, Developing a model for chloride ions transport in cement concrete under dynamic flexural loading and dry-wet cycles, Math. Probl. Eng. 2017 (2017).

[75] W. Zhang, Y. Cai, Basis of anisotropic damage mechanics, Contin. Damage Mech. Numer. Appl, Springer, 2010, pp. 217–355.

[76] C. Wang, Y. Zhang, A. Ma, Investigation into the fatigue damage process of rubberized concrete and plain concrete by AE analysis, J. Mater. Civ. Eng. 23 (2010) 953–960.

[77] N.K. Banjara, K. Ramanjaneyulu, Experimental investigations and numerical simulations on the flexural fatigue behavior of plain and Fiber-reinforced concrete, J. Mater. Civ. Eng. 30 (2018) 04018151.

[78] C. Wang, Y. Zhang, A. Ma, Investigation into the fatigue damage process of rubberized concrete and plain concrete by AE analysis, J. Mater. Civ. Eng. 23 (2010) 953–960.

[79] K.M.A. Sohel, K. Al-Jabri, M.H. Zhang, J.Y.R. Liew, Flexural fatigue behavior of ultra-lightweight cement composite and high strength lightweight aggregate concrete, Constr. Build. Mater. 173 (2018) 90–100, https://doi.org/10.1016/j.conbuildmat.2018.03.276.

[80] S. Seitl, Z. Keršner, V. Bílek, Z. Knésl, Glass fibre reinforced cement based composite: fatigue and fracture parameters, http://dspace5.zcu.cz/handle/11025/1555, (2009) , Accessed date: 19 April 2019.

[81] D.P. Bentz, W.S. Guthrie, S.Z. Jones, N.S. Martys, Predicting service life of steel-reinforced concrete exposed to chlorides, Concr. Int. 36 (2014) 55–64.

[82] P. Soroushian, M. Elzafraney, Damage effects on concrete performance and microstructure, Cem. Concr. Compos. 26 (2004) 853–859, https://doi.org/10.1016/j.cemconcomp.2003.05.001.